Choi, C. E. *et al*. (2016) ***Géotechnique Letters*** **6**, 267–274, http://dx.doi.org/10.1680/jgele.16.00103

Coarse granular flow interaction with slit structures

C. E. CHOI*, G. R. GOODWIN*, C. W. W. NG*, D. K. H. CHEUNG*, J. S. H. KWAN† and W. K. PUN†

Coarse grains accumulate in geophysical flow fronts and have high solid fractions. Such fronts may arch in slit structures such as baffles and slit dams, leading to the rapid trapping of particles and potentially high-energy overflow. Existing empirical slit-structure design recommendations are limited and inadequate since they only focus on the slit size to particle diameter ratio (s/δ) and neglect the pileup height and pre-impact flow energy. Flume modelling was thus adopted to study coarse flow fronts impacting a slit structure. The characteristic Froude conditions, flow particle diameter and the ratio s/δ were varied. Results have shown the pileup height, and hence the confining stress is dependent on Froude conditions, but is not strongly influenced by s/δ. The flow particle diameter influences collisional and frictional stresses and hence the mean outflow rate, which is correlated with pileup height. Grain-trapping efficiency depends on both s/δ and Froude conditions. In contrast to existing continuum-based theory for slit-structure interaction, frictional contacts should be considered for coarse-grained flow fronts. High-energy supercritical flows lead to low trapping efficiency since stable arches cannot form at high shear rates. This implies that multiple slit structures may be more appropriate for attenuating high-energy supercritical flows.

KEYWORDS: landslides; slopes; soil/structure interaction

NOTATION

B	channel width (m)
E	grain-trapping efficiency
$\boldsymbol{g}$	acceleration due to gravity (m/s^2)
h_u	characteristic flow depth (m)
k	constant
N	number of particles in flow
N_{Fr}	Froude number
N_{Sav}	Savage number
Q	slit outflow rate (m^3/s)
Q_C	control outflow rate (m^3/s)
s	slit size (m)
t	time (s)
$\boldsymbol{U}$	bulk flow velocity (m/s)
V	bulk volume of flow (m^3)
Δz_o	pileup height at slit dam (m)
$\dot{\gamma}$	shear rate (/s)
δ	particle diameter (m)
θ	channel inclination (deg)
v_s	solid volume fraction
ρ_s	flow density at slit structure (kg/m^3)
ρ_u	flow density upstream (kg/m^3)
ϕ	grain–base interface friction angle

INTRODUCTION

Coarse grains and boulders accumulate at geophysical flow fronts by way of segregation (Suwa, 1988). Such fronts are highly inertial, potentially incapacitating structures along their flow path and claiming lives (Hungr & Evans, 1988; Ng *et al*., 2016). Zhang *et al*. (1996) reported a boulder-rich debris flow front impacting a reinforced concrete bridge pier on the Chengdu–Kunming Railroad in China, destroying the pier and causing 220 fatalities.

To protect downstream facilities, rigid slit structures such as slit dams (Armanini & Larcher, 2001; Lien, 2003) and baffles (VanDine, 1996) are often installed along predicted flow paths (Figs 1(a) and 1(b)). Slit structures have one or more upward-facing apertures to constrict flows and attenuate energy. Advantageously, small flow events can pass without substantially reducing the retention capacity (Lien, 2003), while larger flow events are arrested. Typical design considerations are grain-trapping efficiency and pileup height (Ng *et al*., 2014) although constriction-induced stable arch formation, potentially leading to trapping of particles and hazardous overflow, is usually ignored.

One approach for calculating the pileup height Δz_0 of a continuum flow at a narrow slit dam was proposed by Armanini & Larcher (2001), and was validated for a solid fraction of up to 0·01, which is substantially lower than the typical solid fraction for dry granular flows, around 0·6 (Denlinger & Iverson, 2001)

$$\frac{\Delta z_0}{h_u} = \frac{3}{2}\left(\frac{N_{Fr}B}{s}\right)^{2/3} - 1 - \frac{N_{Fr}^2}{2}\left\{1 - \left[1 - \frac{2}{3}\left(\frac{N_{Fr}B}{s}\right)^{-(2/3)}\right]^2\right\} \quad (1)$$

where h_u is the upstream flow depth, N_{Fr} is the Froude number, B is the channel width and s is the slit size. This suggests that N_{Fr} and s/B (transverse blockage) are relevant parameters for constricted flow behaviour, although arching effects for small s/δ ratios are not considered.

Small s/δ ratios were considered by Ikeya & Uehara (1980) and Watanabe *et al*. (1980). They carried out small-scale experiments using water and a maximum solid fraction (v_s) of 0·03. They proposed empirical particle trapping criteria for slit dams of $s/\delta_{max} \leq 1{\cdot}5$–$2{\cdot}0$, where δ_{max} is the maximum particle diameter. Similarly, Silva *et al*. (2016) investigated boulder trapping using a maximum mean solid volume

Manuscript received 5 July 2016; first decision 14 September 2016; accepted 27 September 2016.
Published online at www.geotechniqueletters.com on 19 October 2016.
*Department of Civil and Environmental Engineering, Hong Kong University of Science and Technology, Hong Kong, Hong Kong.
†Civil Engineering and Development Department, Hong Kong SAR Government, Hong Kong, Hong Kong.

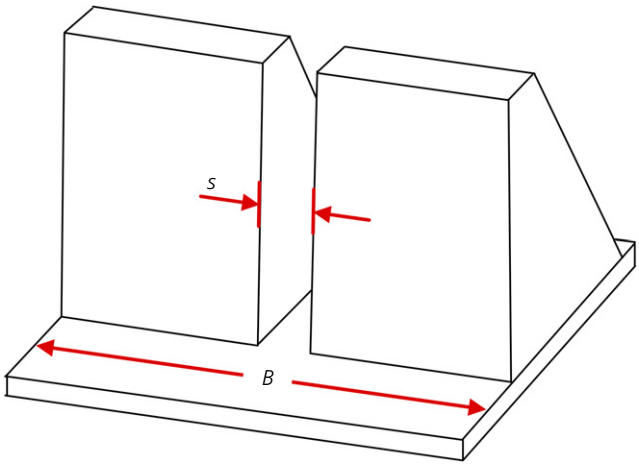

Fig. 1. Schematic diagram of a slit dam

fraction of 0·02, proposing a criterion of $1{\cdot}0 \leq s/\delta_{95} \leq 1{\cdot}4$. Froude similarity with prototype debris flows was achieved in all three studies ($0{\cdot}0 \leq N_{Fr} \leq 5{\cdot}0$; Hübl *et al.*, 2009). For all three studies, the solid volume fraction, a key parameter for characterising channelised flows (Armanini, 2015), was much lower than that of dry granular flows, where v_s is typically around 0·6 (Denlinger & Iverson, 2001). Flows were inviscid, with much lower flow shear strength than the frictional flows presented in this manuscript, with correspondingly different impact characteristics (Choi *et al.*, 2015a).

Other guidelines for fundamentally similar slit structures have also been established empirically. Table 1 summarises mutually inconsistent recommendations for slit dam slit spacing proposed in China (MLR, 2004), Taiwan (SWCB, 2005) and Japan (NILIM, 2007), considering various s/δ_{max} ratios. Furthermore, slit structures are also recommended for use in Canada (VanDine, 1996) and Europe (Jóhannesson *et al.*, 2009), to brake debris flows and snow avalanches, respectively. However, these recommendations are empirical, with no quantitative consideration of the ratio s/δ.

In this experimental study, pileup height and grain-trapping efficiency of slit structures were investigated. Approaching flow Froude conditions (N_{Fr}), flow particle diameter (δ) and the slit size to particle diameter ratio (s/δ) were varied.

FLUME MODELLING

A 5 m long flume model (Choi *et al.*, 2015b) was adopted (Fig. 2(a)). The channel is 200 mm wide and 500 mm deep. The walls and base are made of transparent acrylic channel and are lined with plastic film. The interface friction angle between different sphere sizes and channel walls is given in Table 2. A gate equipped with an electromagnetic lock at the base of the door facilitates dam-break conditions. The gate is loaded using springs attached to the frame of the flume. Upon deactivation of the electromagnetic lock, the spring-loaded gate swings vertically upwards. At the highest point of ascent of the gate, brake pads arrest the gate to prevent it from obstructing the dam break of the granular material from the hopper. Two tall rigid barriers installed side by side inside the channel, 900 mm downstream from the gate, form the slit structure (Fig. 2(b)).

Scaling

Experimental set-up design was guided by using Buckingham Π dimensional analysis (Iverson, 2015). Stable arching requires shear strength, a shear rate and a constriction, so an assembly of spheres on an inclined channel interacting with a slit structure is assumed. Dimensionless groups are then constructed

$$\left(\frac{\boldsymbol{U}}{\sqrt{\boldsymbol{g}h_u \cos\boldsymbol{\theta}}}\right) = f\left(\frac{4\pi N\delta^3}{3V}, \frac{h_u}{\delta}, \frac{B}{\delta}, \frac{s}{\delta}, \frac{\Delta z_0}{h_u}, \frac{Q}{Q_C}, \frac{\rho_s}{\rho_u}, \frac{\delta^2\dot{\gamma}^2}{\boldsymbol{g}h_u \cos\theta}\right) \quad (2)$$

where $\boldsymbol{U}$ is the flow velocity; $\boldsymbol{g}$ is the gravity-induced acceleration; h_u is the upstream flow depth measured perpendicular to the channel bed; θ is channel inclination; N is the number of particles; δ is the characteristic particle diameter; V is bulk volume; B is channel width; s is obstacle slit size; Δz_0 is deposition height at the slit structure; Q and Q_c are slit and control outflow rates, respectively; ρ_u and ρ_s are the bulk density upstream and at the slit, respectively; and $\dot{\gamma}$ is the shear rate.

$\boldsymbol{U}/(\boldsymbol{g}h_u \cos\theta)^{0{\cdot}5}$ is a Froude number (N_{Fr}), $4\pi N\delta^3/3V$ is the solid volume fraction and h_u/δ is the normalised flow depth. These three groups govern flow dynamics for dry granular flows (Armanini *et al.*, 2014; Armanini, 2015). The ratios B/δ, s/δ and $\Delta z_0/h_u$ characterise geometric relationships for slit-structure interaction; Q/Q_C indicates the outflow rate reduction due to the slit structure; ρ_s/ρ_u is post-impact flow compression; and finally, $\delta^2\dot{\gamma}^2/(gh\cos\theta)$ is a Savage number, indicating the extent to which flows are collisional or frictional (Savage, 1984).

Instrumentation

Flow dynamics were captured using two Prosilica GE640 cameras: one facing the side of the slit structure, sampling at 200 FPS (frames per second) and one downstream in-channel sampling at 30 FPS, capturing the entire flow (up to 4 min). A square reference grid (20 mm^2) was imposed on the flume walls.

Testing procedures

Uniform glass spheres of a particular size measuring 40 kg were systematically inserted into the storage area. The initial solid volume fraction is around 0·6, substantially higher than that of flows reported in Ikeya & Uehara (1980) and Watanabe *et al.* (1980) which report a maximum solid volume fraction of 0·03. The material properties are summarised in Table 2. The flume was then inclined using

Table 1. Summary of slit-structure design criteria

Authors	Criteria	Notes
Ikeya & Uehara (1980)	$s/\delta_{max} \leq 1{\cdot}5$–$2{\cdot}0$	Low-concentration sand transport w/ slit dam
Watanabe *et al.* (1980)	$s/\delta_{max} \leq 1{\cdot}5$–$2{\cdot}0$	Low-concentration sand transport w/ slit dam
Silva *et al.* (2016)	$1{\cdot}0 \leq s/\delta_{95} \leq 1{\cdot}4$	Low-concentration boulder transport w/ slit dam
China (MLR, 2004)	$2{\cdot}0 \leq s/\delta_{max} \leq 4{\cdot}5$	Guidelines for slit dams
Japan (NILIM, 2007)	$s/\delta_{95} \sim 1{\cdot}5$	Guidelines for slit dams
Taiwan (SWCB, 2005)	$1{\cdot}5 \leq s/\delta_{max} \lesssim 2{\cdot}0$	Guidelines for slit dams

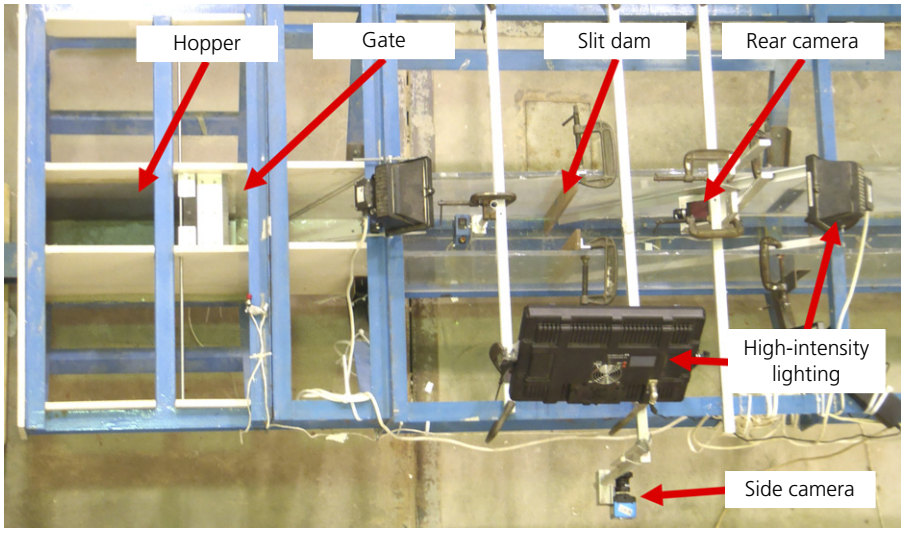

(a)

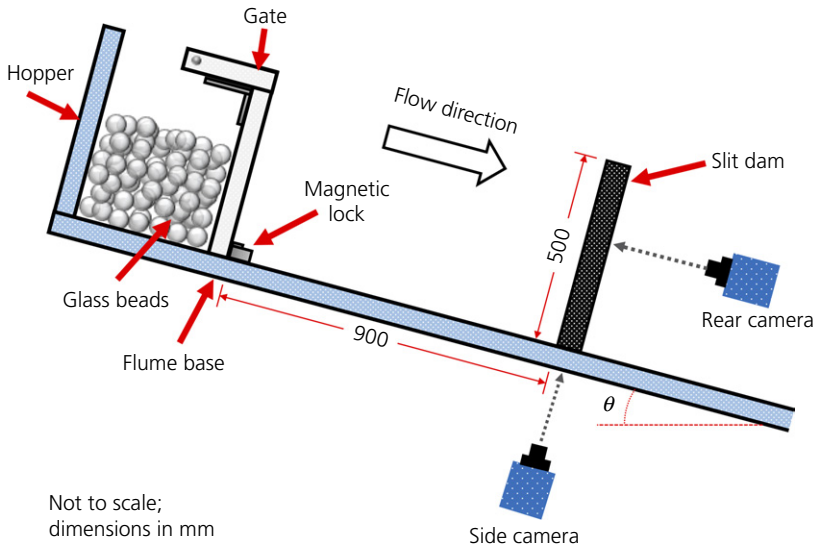

(b)

Fig. 2. (a) Plan view of flume model and instrumentation set-up and (b) side view schematic diagram

Table 2. Material properties

Property	Value		
Particle diameter: mm	9·8	22·5	39·0
Particle-wall friction coefficient: deg	16·6	11·6	11·7
Density: kg/m^3	2630	2630	2630

an overhead crane. Then, the high-speed cameras were synchronously initiated as the gate was opened, allowing grains to flow downstream into the slit structure. After each test, grains trapped upstream were removed from the flume and weighed to calculate the grain-trapping efficiency.

Characterisation of variable quantities

The flow depth h_u, pileup height z_0 and velocity $\boldsymbol{U}$ were measured at the wall based on multiple high-speed images using the square reference grid. The total number of particles in the hopper before initiation, N, was back-calculated using basic geometric considerations from the total mass of the particles and their mean radius. The initial bulk volume V was calculated from the hopper geometry. The initial solid volume fraction v_s could then be calculated from N, V and δ. The downstream change in bulk density ρ_u/ρ_s was assumed to be unity since uniform spheres have a very low degree of compressibility (Iverson, 2015). The grain–base interface angle ϕ was obtained using tilt tests following the procedure outlined in Jiang & Towhata (2013).

Test programme

Channel inclination (θ) was varied from 6° to 30°, particle diameter (δ) was varied as 9·8, 22·5 and 39·0 mm, and the ratio s/δ was varied from 0 (no slit) to 20 (open channel). The open-channel tests allow reliable characterisation of (*a*) the flow front Froude conditions at the point where the slit structure would be and (*b*) the control outflow rate Q_C. Tables 3 and 4 summarise the physical flume tests.

INTERPRETATION OF TEST RESULTS

Observed mechanisms

Figure 3 shows the observed impact mechanisms for test C30-SD50. Dam break occurs at $t = 0{\cdot}0$ s and the flow is released from the hopper (Fig. 3(a)). At $t = 0{\cdot}2$ s,

Table 3. Control test programme for flow characterisation

Test ID	Channel inclination, θ: deg	Particle diameter, δ: mm	Slit opening, s: mm	Slit size to particle size ratio, s/δ	Flow depth to particle size ratio, h_u/δ	Froude number, N_{Fr}	Depth-averaged shear rate: s^{-1}	Depth-averaged Savage number, N_{Sav}
C06-D1	6	9·8	200	20·0	1·7	0·7	3·3	0·006
C10-D1	10	9·8	200	20·0	3·1	1·1	11·0	0·038
C14-D1	14	9·8	200	20·0	4·5	1·3	10·5	0·024
C18-D1	18	9·8	200	20·0	5·5	1·4	10·0	0·019
C22-D1	22	9·8	200	20·0	6·6	1·5	9·2	0·013
C26-D1	26	9·8	200	20·0	7·1	1·9	7·4	0·008
C30-D1	30	9·8	200	20·0	7·4	2·3	8·9	0·012
C06-D2	6	22·5	200	8·9	1·4	0·7	1·6	0·004
C10-D2	10	22·5	200	8·9	1·5	0·9	2·8	0·012
C14-D2	14	22·5	200	8·9	2·2	1·2	4·9	0·026
C18-D2	18	22·5	200	8·9	2·4	1·5	7·0	0·047
C22-D2	22	22·5	200	8·9	3·2	1·5	5·5	0·023
C26-D2	26	22·5	200	8·9	3·4	2·0	8·4	0·050
C30-D2	30	22·5	200	8·9	3·8	2·5	7·7	0·034
C06-D4	6	39·0	200	5·1	1·0	0·3	—	—
C14-D4	14	39·0	200	5·1	1·8	1·0	2·5	0·015
C18-D4	18	39·0	200	5·1	1·8	1·2	4·1	0·038
C22-D4	22	39·0	200	5·1	2·3	1·6	6·6	0·081
C26-D4	26	39·0	200	5·1	2·5	1·6	6·0	0·065
C30-D4	30	39·0	200	5·1	2·7	2·0	5·4	0·050

Table 4. Main flume test programme

Test ID	Channel inclination, θ: deg	Slit opening, s: mm	Particle diameter, δ: mm	Slit size to particle size ratio, s/δ	Flow depth to particle size ratio, h_u/δ	Froude number, N_{Fr}
C06-D1-SD0	6	0	9·8	—	1·7	0·7
C10-D1-SD0	10	0	9·8	—	3·1	1·1
C14-D1-SD0	14	0	9·8	—	4·5	1·3
C18-D1-SD0	18	0	9·8	—	5·5	1·4
C30-D1-SD0	30	0	9·8	—	7·4	2·3
C06-D1-SD2	6	20	9·8	2·0	1·7	0·7
C10-D1-SD2	10	20	9·8	2·0	3·1	1·1
C14-D1-SD2	14	20	9·8	2·0	4·5	1·3
C18-D1-SD2	18	20	9·8	2·0	5·5	1·4
C22-D1-SD2	22	20	9·8	2·0	6·6	1·5
C26-D1-SD2	26	20	9·8	2·0	7·1	1·9
C30-D1-SD2	30	20	9·8	2·0	7·4	2·3
C06-D1-SD3	6	30	9·8	3·0	1·7	0·7
C10-D1-SD3	10	30	9·8	3·0	3·1	1·1
C14-D1-SD3	14	30	9·8	3·0	4·5	1·3
C18-D1-SD3	18	30	9·8	3·0	5·5	1·4
C30-D1-SD3	30	30	9·8	3·0	7·4	2·3
C06-D1-SD4	6	40	9·8	4·0	1·7	0·7
C10-D1-SD4	10	40	9·8	4·0	3·1	1·1
C14-D1-SD4	14	40	9·8	4·0	4·5	1·3
C18-D1-SD4	18	40	9·8	4·0	5·5	1·4
C30-D1-SD4	30	40	9·8	4·0	7·4	2·3
C06-D1-SD5	6	50	9·8	5·0	1·7	0·7
C10-D1-SD5	10	50	9·8	5·0	3·1	1·1
C14-D1-SD5	14	50	9·8	5·0	4·5	1·3
C18-D1-SD5	18	50	9·8	5·0	5·5	1·4
C30-D1-SD5	30	50	9·8	5·0	7·4	2·3
C06-D1-SD8	6	80	9·8	8·0	1·7	0·7
C30-D1-SD8	30	80	9·8	8·0	7·4	2·3
C06-D1-SD10	6	100	9·8	10·0	1·7	0·7
C30-D1-SD10	30	100	9·8	10·0	7·4	2·3
C06-D2-SD2	6	40	22·5	1·8	1·4	0·7
C10-D2-SD2	10	40	22·5	1·8	1·5	0·9
C14-D2-SD2	14	40	22·5	1·8	2·2	1·2
C18-D2-SD2	18	40	22·5	1·8	2·4	1·5
C22-D2-SD2	22	40	22·5	1·8	3·2	1·5
C26-D2-SD2	26	40	22·5	1·8	3·4	2·0
C30-D2-SD2	30	40	22·5	1·8	3·8	2·5
C06-D4-SD2	6	80	39·0	2·1	1·0	0·3
C14-D4-SD2	14	80	39·0	2·1	1·8	1·0
C18-D4-SD2	18	80	39·0	2·1	1·8	1·2
C22-D4-SD2	22	80	39·0	2·1	2·3	1·6
C26-D4-SD2	26	80	39·0	2·1	2·5	1·6
C30-D4-SD2	30	80	39·0	2·1	2·7	2·0

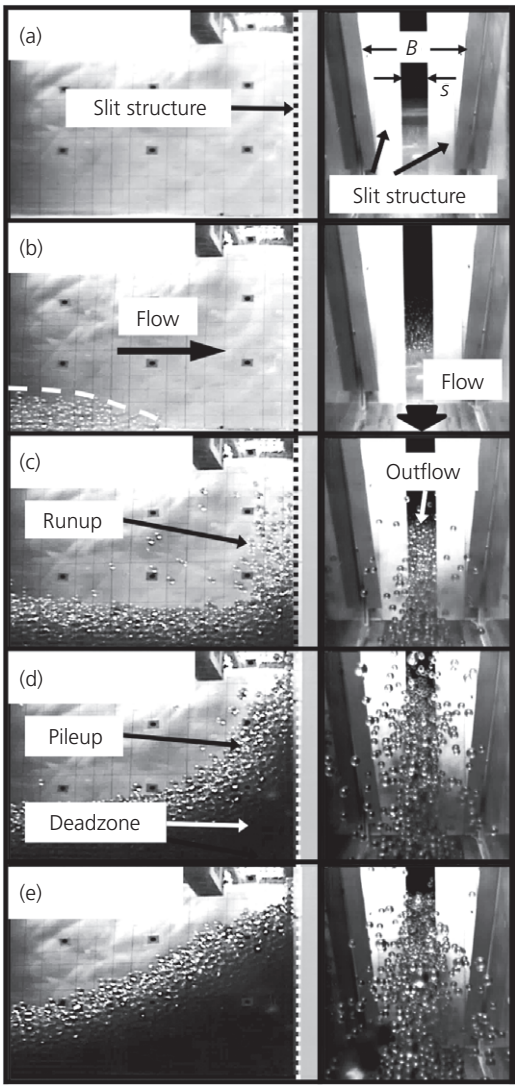

Fig. 3. Observed slit-structure flow kinematics for supercritical flow from side and downstream cameras (test C30-D1-SD5, wherein $B = 200$ mm and $s = 50$ mm): (a) $t = 0{\cdot}0$ s; (b) $t = 0{\cdot}2$ s; (c) $t = 0{\cdot}4$ s; (d) $t = 0{\cdot}6$ s; (e) $t = 0{\cdot}8$ s

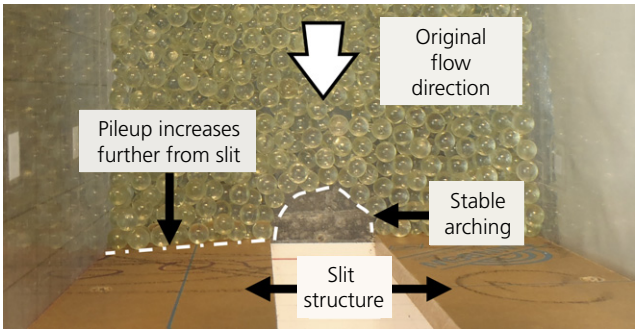

Fig. 4. Plan view of stable arch formation behind the slit structure (test C06-SD50)

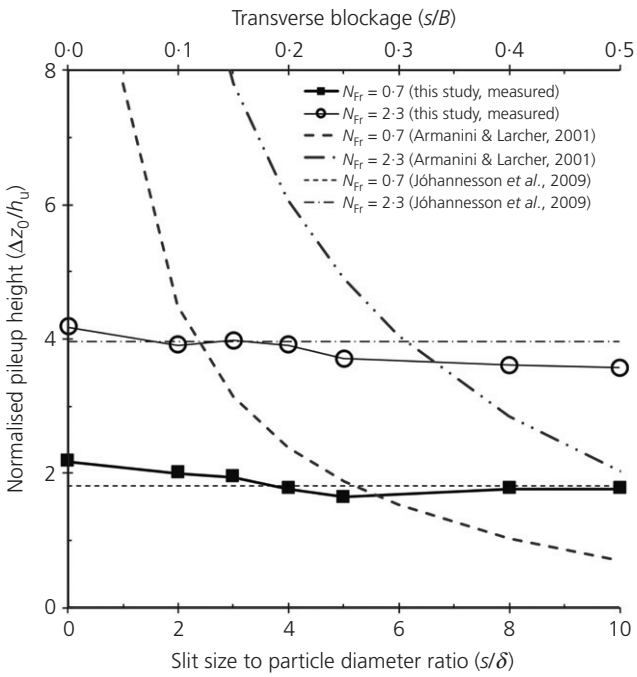

Fig. 5. Measured and theoretical pileup heights from slit-structure interaction

a supercritical ($N_{Fr} = 2{\cdot}3$) wedge-shaped flow front appears (Fig. 3(b)). This flow front is friction dominated ($N_{Sav} \sim 0{\cdot}01$), with an estimated volume fraction of 0·5–0·6. Later, at $t = 0{\cdot}4$ s (Fig. 3(c)), impact with the slit structure occurs: particles run up the slit structure (similar to water; c.f. Choi *et al.*, 2015a) and discharge through the slit. Figs 3(d) and 3(e) show particles piling up; this pileup was almost static near the channel side-walls, where a ramp-like dead zone forms. The outflow of the material suggests that single slit structure may not be appropriate for flow control since particles saltate dangerously at initial outflow. Secondary structures may be required to control such saltating material. Figure 4 shows a typical arrested flow for test C06-SD50, with a stable arch highlighted. For all tests in this study stable arches were formed around the slit opening, suggesting that the minimum stable arch length must always be longer than the opening. It is also observed that the pileup height Δz_0 is highest at the wall and decreases nearer the slit. Values quoted later in this manuscript are maxima, measured at the wall.

Pileup height at slit structure

Slit-structure height is a key design consideration: slit-structure height must be taller than pileup height if hazardous overflow is to be avoided (Choi *et al.*, 2014). Figure 5 shows the normalised deposition height at the slit structure ($\Delta z_0/h_u$) against s/δ (proportional to s/B) and N_{Fr}. Experimental data from this study is compared with the theory from Armanini & Larcher (2001) (equation (1)) and of Jóhannesson *et al.* (2009) (equation (3)), both of which are computed using experimentally attained Froude numbers

$$2N_{Fr}^2 + 1 = \frac{\rho_s}{\rho_u}\left(\frac{\Delta z_0}{h_u}\right) - \frac{\Delta z_0}{h_u} + \left(\frac{\rho_s}{\rho_u}\frac{\Delta z_0}{h_u}\right)^{-1} \quad (3)$$

Equation (1) assumes an incompressible two-phase flow (i.e. a wet granular flow) on a shallow inclination (< 6°) interacting with a narrow slit dam where energy is conserved. It is a function of the Froude number and the ratio between channel width and slit width and has been validated for sediment transport problems with a maximum solid volume fraction of 0·01. Equation (3) assumes a dry compressible continuum flow (i.e. dry granular flow) impacting a continuous rigid barrier. It considers conservation of momentum, a reflective dynamic impact force and, advantageously for granular materials, compressibility. Uniform spheres have low bulk compressibility, so it is assumed in this analysis that compressibility $\rho_s/\rho_u = 1$. Disadvantageously,

neither approach considers granular properties such as particle diameter δ, despite their relevance to granular slit problems (c.f. Ikeya & Uehara, 1980).

For both theoretical approaches, an increase of N_{Fr} increases $\Delta z_0/h_u$ (consistent with Armanini *et al.*, 2011; Choi *et al.*, 2015a). Furthermore, equation (1) suggests $\Delta z_0/h_u$ should decrease with transverse blockage: the wider the slit, the more the material that can pass through it.

In contrast, experimental data has shown that the normalised maximum pileup height at the channel wall is not strongly influenced by s/δ for the range considered. This is attributed to the shear resistance mobilised as particles rearrange due to the applied effective stress (Terzaghi, 1943), causing arch formation. Arches tend to retard or halt motion (Janda *et al.*, 2008), but this is not considered in equation (1). The normalised maximum pileup height approaches that of equation (3) since the edge of the slit structure acts like a continuous barrier. Similar to the theoretical predictions of equation (3), variation in N_{Fr} causes a change in pileup height. N_{Fr} should thus be a major consideration for structure height for coarse-grained fronts, while s/δ is evidently less important.

Pileup height and outflow rate

Figure 6 shows the normalised pileup height $\Delta z_0/h_u$ against the normalised mean outflow rate Q/Q_C. Outflow rates were computed using the time from initial impact to cessation of flow and the measured retained volume. Three particle diameters were used; the ratio s/δ for each is around 2·0. Multiple channel inclinations were used, controlling N_{Fr} and hence $\Delta z_0/h_u$. The depth-averaged Savage number N_{Sav} was used to characterise the flow regime. The Savage number relies on shear rate and flow depth, and assumes open-channel flow. Relevant quantities were measured near the flow front from each test at 900 mm downstream (where the barrier would otherwise be installed), and are recorded in Table 3. The shear rate was calculated using an average of the velocity of the top and bottom layers of the flow front, and the flow depth.

The number of particle diameters per unit depth reduces with increasing particle diameter. A low number of particles depthwise can lead to saltation and highly collisional flow (Bryant *et al.*, 2015). This appears to be linked with the pileup height: the 9·8 mm particles have the highest normalised pileup height since they are less collisional ($0{\cdot}007 < N_{Sav} < 0{\cdot}038$), allowing frictional contacts to retard motion pre-outflow; by contrast, the 39 mm particles ($0{\cdot}015 < N_{Sav} < 0{\cdot}081$) are more collisional, tending to barge energetically downstream before full pileup can occur. The normalised outflow rate for these two sizes is 2–5 and 10–20%, respectively. This is again attributed to variation of N_{Sav}, altering the degree to which the flow is frictional or collisional, suggesting that the flow particle diameter is a key parameter. Additionally, higher pileups are linked with lower outflow rates, suggesting that confining stress promotes stable arch formation (c.f. Cleary *et al.*, 1979). However, the results differ from incompressible fluid mechanics predictions for open-channel flow

$$\frac{1}{2}\rho \boldsymbol{U}^2 + \rho \boldsymbol{g} h_u = k \tag{4}$$

where k is a constant. Equation (4) suggests that the flow rate is constant both before and after the slit. By contrast, the outflow rate for dry granular flows in this study was not constant before and after the slit: the downstream flow rate was between 78 and 98% less than the upstream. This suggests that resisting shear forces mobilised by frictional contacts should not be ignored in slit-structure analyses for coarse-grained flows.

Grain-trapping efficiency

Figure 7 shows the grain-trapping efficiency (E) as functions of s/δ and characteristic N_{Fr}. Grain-trapping efficiency is defined as the number of grains remaining upstream of the slit structure following flow arrest. Grain-trapping efficiency increases with both increasing N_{Fr} and s/δ, which can be linked with the continuous dynamic formation and destruction of arches within flows. Arch strength evidently depends on shear rate: supercritical flow particles are highly inertial and break stable arches easily. Additionally, high N_{Fr} increases runup/pileup height (Choi *et al.*, 2015a), increasing the number of stable arches required for total flow arrest.

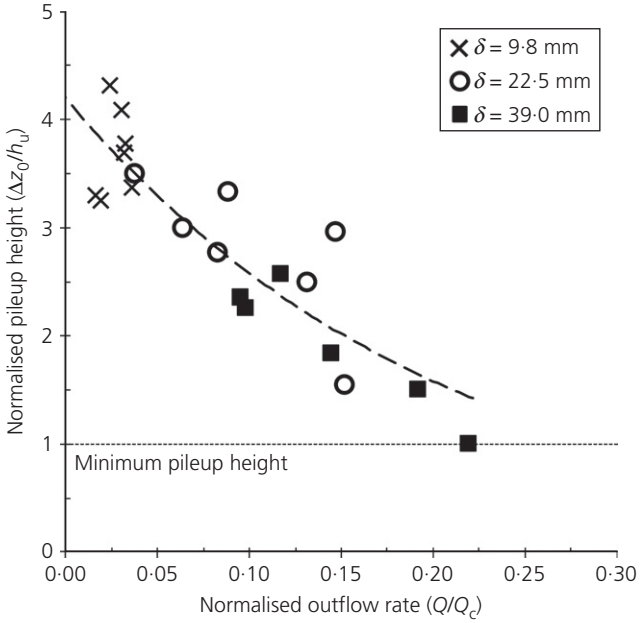

Fig. 6. Measured relationship between particle size, pileup height and outflow rate

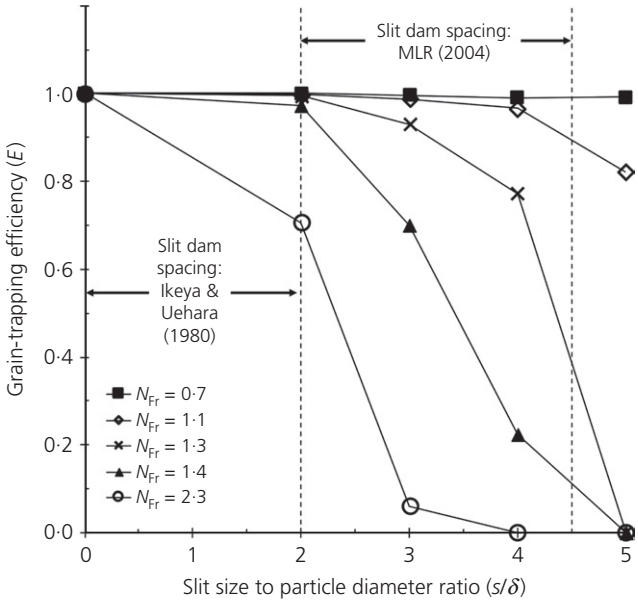

Fig. 7. Measured relationship between s/δ, Froude conditions and grain-trapping efficiency

Arch strength is also affected by its length (Pardo & Sáez, 2014): shorter arches are generally stronger, so higher stresses can be sustained in constrictions. The probability of formation of stable arches thus increases as s/δ decreases (Janda *et al.*, 2008).

It should be noted that an assembly of monosised spheres does not have an elastic compressibility component: volume change is necessarily facilitated by irreversible slippage at intergrain contacts (Iverson, 2015). By contrast, non-spherical particles are able to accommodate porosity change and particle interlocking. Compression tends to increase bulk stiffness (Iverson, 1997), from which it may be inferred that there would be less relative intergrain displacement and thus forming stronger arches for non-spherical particles. It is anticipated that this would increase the grain-trapping efficiency compared with an equivalent assembly of spheres, so the results in this paper are likely to be conservative.

Although slit dams are often designed for full retention of coarse-grained flow fronts, for $N_{Fr} = 2{\cdot}3$ and $s/\delta = 2{\cdot}0$ (Ikeya & Uehara, 1980), grain retention is just 70% since N_{Fr} is relatively high. Similarly, the Ministry of Land and Resources for the People's Republic of China proposes an upper bound of $s/\delta = 4{\cdot}0$ (MLR, 2004). For this value, N_{Fr} has a significant effect on trapping efficiency due to the varying Froude conditions. Effective slit design should therefore consider N_{Fr} in addition to s/δ.

CONCLUSIONS

A series of flume experiments studying the impact of dry coarse-grained flows impacting a slit structure for varying Froude conditions (N_{Fr}), particle diameter (δ) and ratio of slit size to particle diameter (s/δ) was carried out. Results from this study show the following.

- The pileup height, and hence the confining stress, is dependent on Froude conditions, but is not strongly influenced by s/δ. Froude conditions determine the energy available for pileup and should be considered in slit-structure design.
- The flow particle diameter influences collisional and frictional stresses and hence the mean outflow rate. Outflow rate is correlated with pileup height. This suggests that flow particle diameter is another key design consideration.
- Results from this study contrast with existing continuum-based slit-dam theory. Such theory does not consider frictional contacts characteristic of coarse-grained frictional flow fronts or the role of the pileup height (and hence confining stress) for promoting stable arch formation.
- Grain-trapping efficiency depends on both s/δ and Froude conditions. High-energy supercritical flows lead to dangerous grain saltation and low trapping efficiency since stable arches cannot form at high shear rates. This implies that multiple slit structures are required to catch material from high-energy supercritical flows rather than allowing the saltation of grains freely downstream.

ACKNOWLEDGEMENTS

The authors are grateful for the financial support from the theme-based research grant T22-603/15N provided by the Research Grants Council of the Government of Hong Kong Special Administrative Region, China. This paper is published with the permission of the Head of the Geotechnical Engineering Office and the Director of Civil Engineering and Development, the Government of Hong Kong Special Administrative Region. The authors also acknowledge the support of the HKUST Jockey Club Institute for Advanced Study.

REFERENCES

Armanini, A. (2015). Closure relations for mobile bed flows in a wide range of slopes and concentrations. *Adv. Water Resour.* **81**, 75–83.

Armanini, A. & Larcher, M. (2001). Rational criterion for designing opening of slit check dam. *J. Hydraul. Engng, ASCE* **127**, No. 2, 94–104.

Armanini, A., Larcher, M. & Odorizzi, M. (2011). Dynamic impact of a debris flow front against a vertical wall. In *5th international conference on debris-flow hazards. Mitigation, mechanics, prediction and assessment* (eds R. Genevois, D. L. Hamilton and A. Prestininzi), Padua, Italy, pp. 1041–1049. Rome, Italy: Casa Editrice Università La Sapienza.

Armanini, A., Larcher, M., Nucci, E. & Dumbser, M. (2014). Submerged granular channel flows driven by gravity. *Adv. Water Resour.* **63**, 1–10.

Bryant, S. K., Take, W. A., Bowman, E. T. & Millen, M. D. L. (2015). Physical and numerical modelling of dry granular flows under Coriolis conditions. *Géotechnique* **65**, No. 3, 188–200, http://dx.doi.org/10.1680/geot.13.P.208.

Choi, C. E., Ng, C. W. W., Song, D., Kwan, J. S. H., Shiu, H. Y. K., Ho, K. K. S. & Koo, R. C. H. (2014). Flume investigation of landslide debris baffles. *Can. Geotech. J.* **51**, No. 5, 540–533.

Choi, C. E., Au-Yeung, S. C. H. & Ng, C. W. W. (2015a). Flume investigation of landslide granular debris and water runup mechanisms. *Géotech. Lett.* **5**, No. 1, 28–32, http://dx.doi.org/10.1680/geolett.14.00080.

Choi, C. E., Ng, C. W. W., Au-Yeung, S. C. H. & Goodwin, G. R. (2015b). Froude scaling of landslide debris in flume modelling. *Landslides* **12**, No. 6, 1197–1206.

Cleary, M. P., Melvan, J. J. & Kohlhaas, C. A. (1979). The effect of confining stress and fluid properties on arch stability in unconsolidated sands. In *54th Annual Fall Technical Conference and Exhibition of the Society of Petroleum Engineers of AIME, Las Vegas, NV, USA*, paper SPE 8426. Richardson, TX, USA: Society of Petroleum Engineers.

Denlinger, R. P. & Iverson, R. M. (2001). Flow of variably fluidized granular masses across three-dimensional terrain 2. Numerical predictions and experimental tests. *J. Geophys. Res.* **106**, No. B1, 533–566.

Hübl, J., Suda, J., Proske, D., Kaitna, R. & Scheidl, C. (2009). Debris flow impact estimation. In *Proceedings of the 11th international symposium on water management and hydraulic engineering, Ohrid, Macedonia* (eds C. Popovska and M. Jovanovski), pp. 1–5. Skopje, Macedonia: University of Ss Cyril and Methodius.

Hungr, O. & Evans, S. G. (1988). Engineering evaluation of fragmental rockfall hazards. In *Landslides, proceedings of the 5th international symposium on landslides*, Lausanne, Switzerland (ed. C. Bonnard), vol. 1, pp. 685–690. Rotterdam, the Netherlands: Balkema.

Ikeya, H. & Uehara, S. (1980). Experimental study about the sediment control of slit Sabo dams. *J. Japan Erosion Control Engng Soc.* **114**, No. 3, 37–44 (in Japanese).

Iverson, R. M. (1997). The physics of debris flows. *Rev. Geophys.* **35**, No. 3, 245–296.

Iverson, R. M. (2015). Scaling and design of landslide and debris-flow experiments. *Geomorphology* **244**, 9–20.

Janda, A., Zuriguel, I., Garcimartín, A., Pugnaloni, L. A. & Maza, D. (2008). Jamming and critical outlet size in the discharge of a two-dimensional silo. *Europhys. Lett.* **84**, 44002.

Jiang, Y. & Towhata, I. (2013). Experimental study of dry granular flow and impact behavior against a rigid retaining wall. *Rock Mech. Rock Engng* **46**, No. 4, 713–729.

Jóhannesson, T., Gauer, P., Issler, D. & Lied, K. (2009). *The design of avalanche protection dams recent practical and theoretical developments*. Brussels, Belgium: European Commission.

Lien, H. P. (2003). Design of slit dams for controlling stony debris flows. *Int. J. Sediment Res.* **18**, No. 1, 74–78.

MLR (Ministry of Land and Resources) (2004). *Design standards for debris flow hazard mitigation measures (DZ/T0239-2004)*. Beijing, China: Chinese Geological Survey, Ministry of Land and Resources (in Chinese).

Ng, C. W. W., Choi, C. E., Song, D., Kwan, J. S. H., Shiu, H. Y. K., Ho, K. K. S. & Koo, R. C. H. (2014). Physical modelling of baffles influence on landslide debris mobility. *Landslides* **12**, No. 1, 1–18.

Ng, C. W. W., Choi, C. E., Su, A. Y., Kwan, J. S. H. & Lam, C. (2016). Large-scale successive impacts on a rigid barrier shielded by gabions. *Can. Geotech. J.* **53**, No. 10, 1688–1699.

NILIM (National Institute for Land and Infrastructure Management) (2007). *Manual of technical standards for designing sabo facilities against debris flow and Driftwood*, Technical Note of NILIM No. 365. Tsukuba, Japan: Natural Institute for Land and Infrastructure Management, Ministry of Land, Infrastructure and Transport (in Japanese).

Pardo, G. S. & Sáez, E. (2014). Experimental and numerical study of arching soil effect in coarse sand. *Comput. Geotech.* **57**, 75–84.

Savage, S.B. (1984). The mechanics of rapid granular flows. *Adv. Appl. Mech.* **24**, 289–366.

Silva, M., Costa, S., Canelas, R. B., Pinheiro, A. N. & Cardoso, A. H. (2016). Experimental and numerical study of slit-check dams. *Int. J. Sustain. Dev. Plan.* **11**, No. 2, 107–118.

Suwa, H. (1988). *Focusing mechanism of large boulders to a debris-flow front*. PhD thesis, Tokyo University, Japan.

SWCB (Soil and Water Conservation Bureau) (2005). *Soil and water conservation handbook*. Nantou, Taiwan: Soil and Water Conservation Bureau of the Council of Agriculture, Executive Yuan and Chinese Soil and Water Conservation Society (in Chinese).

Terzaghi, K. (1943). Arching in ideal soils. In *Theoretical Soil Mechanics*. Hoboken, NJ, USA: Wiley.

VanDine, D. F. (1996). *Debris flow control structures for forest engineering*. (Ministry of Forests Research Program, Working Paper 22/1996). Vancouver, Canada: Government of the Province of British Columbia.

Watanabe, M., Mizuyama, T. & Uehara, S. (1980). Review of debris flow countermeasure facilities. *J. Japan Erosion Control Engng Soc.*, **115**, No. 5, 40–45 (in Japanese).

Zhang, S., Hungr, O. & Slaymaker, O. (1996). The calculation of impact force of boulders in debris flow. In *Debris flow observation and research* (ed. R. Du), pp. 67–72. Beijing, China: Science Press.